ChemistrySelect

Research Article
doi.org/10.1002/slct.202202292

Chemistry Europe
European Chemical Societies Publishing

www.chemistryselect.org

A Combined Study on Degradation Mechanism of Reactive Orange 16 through Fenton-like Process: Experimental Studies and Density Functional Theoretical Findings

Sayiter Yildiz,*[a] Gamze Topal Canbaz,*[b] Savaş Kaya,*[c] and Mikhail M. Maslov*[d]

In this study, the removal efficiency of Reactive orange 16 (RO16) azo dyes from aqueous solution with different Fenton reactions (Fenton/photo-Fenton/sono-Fenton/ sono-photo-Fenton) were investigated. For optimum conditions, the effects of variables such as H_2O_2, Fe^{2+}, reaction time, pH and dye concentration on the oxidation process were investigated. In addition, the interaction between Fenton reagents and the dye molecule was revealed by Density Functional Theory (DFT) calculations. Important quantum chemical parameters reflecting the reactivity of the studied dye were calculated. Effective RO16 degradation was achieved by Fenton oxidation at conditions of 100 mg L^{-1} H_2O_2, 10 mg L^{-1} Fe^{2+}, 100 mg L^{-1} dye concentration, 3 pH and 30 minutes. While the degradation efficiency with Fenton process was 97.77%, it reached 98.78%, 98.31% and 98.22% when UV–A, UV–B and UV–C lights were applied respectively. In the sono-Fenton process application, the degradation efficiency was determined as 97.96%. The degradation of RO16 by sono-photo-Fenton was 96.12%, 96.13% and 96.83% under different lamps (UV–A, UV–B and UV–C), respectively. In addition, in the kinetic study, it was determined that each process complies with the zeroth-order kinetics. To see the nature and power of the interaction between hydroxyl radical and RO16, important quantum chemical parameters of Conceptual Density Functional Theory were calculated and their effects on degradation process were discussed as detailed. Degradation mechanism was highlighted in the light of DFT calculations.

Introduction

Contamination of water with toxic dyes can cause significant environmental problems.[1] Waste waters from textile industries affect aquatic flora and fauna after discharge into the receiving environment. Azo dyes, which are among the micro-pollutants, pose a great threat to the environment and public health due to their toxic nature.[2] Some azo dyes are known to be toxic and carcinogenic.[3] Reactive dyes are water soluble, biodegradable and form a strong complex (with salts or metals)[4] Reactive orange 16 (RO16) is one of the most produced and used reactive azo dyes among different dye types.[5]

Considering the negative impact of azo dye molecules on the environment, it is important to remove these pollutants from wastewater. For this, different techniques have been proposed such as photochemical, electrochemical and photocatalytic processes,[6–8] biological treatment,[9,10] adsorption,[11–13] LED and ultrasound,[14] filtration,[15] and Fenton reactions.[16–18]

Advanced oxidative processes (AOPs) are promising techniques used to remove various organic compounds. Fenton reaction, one of the AOPs, has been an interesting alternative due to its high efficiency at room temperature, easy use, easily accessible reagents, fast reactions and short treatment times.[19]

Fe^{2+} and hydrogen peroxide (H_2O_2) are mostly used as Fenton reagents due to their many advantages such as cost-effectiveness, non-toxicity and homogeneous catalytic structure.[20,21] During the degradation of hydrogen peroxide catalyzed by Fe^{2+}, hydroxyl radicals ($^{\bullet}OH$) are formed.[22] This process is environmentally friendly for treatment, as no harmful chemical reagents that can be hazardous to the environment are used for $^{\bullet}OH$ production.[23] When divalent iron becomes trivalent during the reaction, the oxidative activity of the Fe^{2+}/H_2O_2 system is significantly reduced. If the trivalent iron is converted back to the divalent state by light radiation (UV/VIS) (photo Fenton), the efficiency and productivity of the method can be significantly increased.[24]

Researchers have applied different methods for RO16 removal. Ruscasso et al.[25] aimed at studying RO16 dye biodegradation by the Antarctic yeast Candida sake 41E. Dye decolorization reached 94.3% within 48 h. Ahmad et al.[26] used Micellar-enhanced ultrafiltration to remove RO16 from aqueous solution, and achieved 99.6% removal efficiency. Abdulhameed et al.[27] preferred the adsorption method for RO16 removal. In this work was used a hybrid nanocomposite biomaterial of crosslinked chitosan-tripolyphosphate/TiO2 nanocomposites, and achieved 92.7% removal efficiency. The other research work used carbon from Phyllanthus reticulatus plant to remove

[a] *Dr. S. Yildiz*
Sivas Cumhuriyet University, Engineering Faculty, Department of Environmental Engineering, 58140, Sivas, Turkey
E-mail: sayildiz@cumhuriyet.edu.tr
[b] *Dr. G. Topal Canbaz*
Sivas Cumhuriyet University, Engineering Faculty, Department of Chemical Engineering, 58140, Sivas, Turkey
E-mail: gtopal@cumhuriyet.edu.tr
[c] *Dr. S. Kaya*
Sivas Cumhuriyet University, Health Services Vocational School, Department of Pharmacy, 58140, Sivas/Turkey
E-mail: savaskaya@cumhuriyet.edu.tr
[d] *Dr. M. M. Maslov*
Department of Condensed Matter Physics, National Research Nuclear University "MEPhI", Kashirskoe Shosse 31, Moscow 115409, Russia
E-mail: MMMaslov@mephi.ru
sayiteryildiz@gmail.com

RO 16 from aqueous media. In this study, maximum dye adsorption was found to be 85.10%.[28] In a different study, ozonation followed by biological treatment in an aerobic MBBR was investigated for degradation of RO16. In the study, at least 97% color degradation was achieved.[29]

No study has been found in the literature on the use of different Fenton-like processes together and examining their synergistic effects for RO16 removal. In addition, many studies have examined the removal efficiency, but have not revealed the interaction between Fenton reagents and dye molecules. In such studies, the highlighting of degradation mechanism for the studied dyes is quite important. For this aim, Density Functional Theory (DFT) based calculations are widely preferred. Density Functional Theory considers the electron density to describe the chemical reactivity of the studied chemical systems. Conceptual Density Functional Theory is a useful tool for the prediction of local and global reactivities of chemical systems.

The aim of this study; i) To investigate the removal efficiency of RO16 azo dyes selected as the target pollutant from aqueous solution by different Fenton reactions (Fenton/ photo Fenton/sono Fenton/ sono photo Fenton) ii) To reveal the interaction phenomenon between Fenton reagents and dye molecule by making DFT calculations. For process performance, the effects of variables such as H_2O_2, Fe^{2+}concentrations, reaction time, pH and dye concentration on the oxidation process were investigated. Moreover we calculated important quantum chemical parameters reflecting the reactivity of the studied dye and discussed the nature and power of the interactions between studied dye and hydroxyl radical through these parameters. This study is very important especially in terms of revealing the synergistic effect of these processes in an integrated reactor and examining the interaction between Fenton reagents and dye molecules by DFT. In the study, the experiments were performed three times and the average values of the samples were taken. The data presented are the mean values obtained in the experiments, standard deviation ($\leq 3\%$) and error bars are indicated in the figures.

Results and Discussion

Optimization of the operating parameters

Initially, the experiments were carried out under the following conditions: (i) dye + Fe^{2+} + H_2O_2 (FP), (ii) dye + Fe^{2+} + H_2O_2 + UV (P-FP), (iii) dye + Fe^{2+} + H_2O_2 + US (S-FP), (iv) dye + Fe^{2+} + H_2O_2 + UV + US (S–P–FP).

The degradation of the dye is mainly due to the hydroxyl radical (•OH) produced by the chemical and photochemical reactions of each process.[30] The •OH produced in Fenton process (FP) results from the iron-catalyzed decomposition of H_2O_2 (Eq. 1).[31]

$$Fe^{2+} + H_2O_2 \rightarrow {}^{\bullet}OH + Fe^{3+} + OH^- \quad (1)$$

In the photo Fenton (P-FP) process, in addition to Equation 15, •OH formation also occurs with the reactions given in Equations 2 and 3:[30]

$$H_2O_{2+}UV \rightarrow {}^{\bullet}OH + {}^{\bullet}OH \quad (2)$$

$$Fe^{3+} + H_2O + UV \rightarrow {}^{\bullet}OH + Fe^{2+} + H^+ \quad (3)$$

Sono photo Fenton (S–P-FP) is the process in which ultrasonic (US), ultraviolet radiation (UV) and Fenton are used together. In this process, •OH production in the aqueous system increases with Fe^{2+} regeneration. In addition to the above reactions, the sono photo fenton process is defined by Equation 4–6.[52]

$$H_2O_2+))) \rightarrow {}^{\bullet}OH + H^{\bullet} \quad (4)$$

$$O_2+))) \rightarrow 2O^{\bullet} \quad (5)$$

$$O^{\bullet} + H_2O+))) \rightarrow 2OH^{\bullet} \quad (6)$$

Here ")))" represents the sonication wave.

Effect of pH

The pH of the solution is an important parameter for FP as the •OH concentration controls the production rate and the iron species in the solution.[33] To determine the effect of pH on the degradation efficiency of RO16, the pH range of 2–7 was investigated. Other parameters were; 10 mg L^{-1} Fe^{2+}, 100 mg L^{-1} H_2O_2, 30 minutes of retention time and 100 mg L^{-1} of dye. The pH-dependent RO16 degradation efficiency results are given in Figure 1.

As seen in Figure 1, while the highest degradation efficiency was obtained at pH 3, there was no significant change in other pH values. RO16 degradation efficiency was 94.3% at pH 2, 97.77% at pH 3, 95.27 at pH 5 and 94.41% at pH 7. Some reduction in degradation above pH 3 is due to the coagulation of the Fe^{3+} formed during the reaction.[34] As precipitate $Fe(OH)_3$ is formed when the pH is above 3, •OH radical production decreases (Eq. 7). Following this precipitation, Fe^{2+} production from Fe^{3+} stops, and then the •OH radical production decreases.[35] In addition, as the pH increases, the self-decomposition rate of H_2O_2 also increases (Eq. 8).[36] At low pH, the removal rate is limited due to the hydroxyl radical scavenging effects of the H^+ ion (Eq. 9).[37]

$$Fe^{3+} + 3OH^{-} \rightarrow Fe(OH)_3 \quad (7)$$

$$H_2O_2 \rightarrow 2H_2O + O_2 \quad (8)$$

$${}^{\bullet}OH + H^+ + e^- \rightarrow H_2O \quad (9)$$

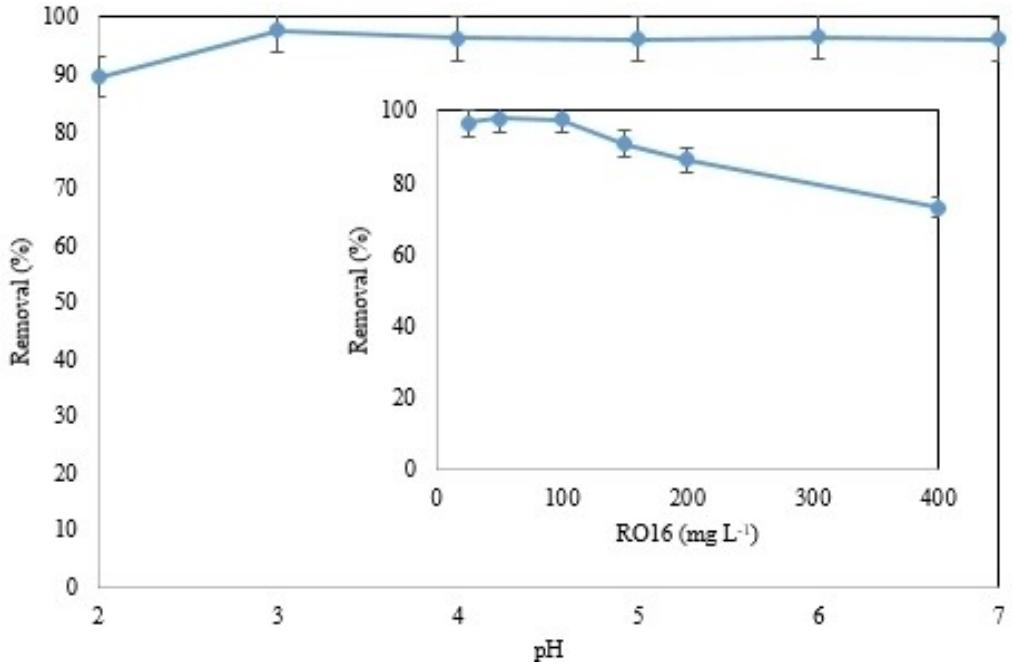

Figure 1. Effect of pH and concentration on RO16 degradation.

Effect of dye concentration

To determine the effect of RO16 concentration on degradation efficiency (Figure 1), different concentrations of the dye (25, 50, 100, 150, 200, 400 mg L^{-1}) was investigated with conditions of 10 mg L^{-1} Fe^{2+}, 100 mg L^{-1} H_2O_2, t 30 min, pH 3. The $^{\bullet}OH$ concentration formed in Fenton-like processes remains constant for all dye concentrations in the medium. With an increase in dye concentration, the rate of degradation decreases under the constant $^{\bullet}OH$ concentration. In the study, the degradation efficiency was determined as 95.27% at 25 mg L^{-1} concentration, 97.77% at 100 mg L^{-1} concentration, and 86.23% and 76.54% for 200 and 400 mg L^{-1} concentration, respectively. Decreased removal efficiencies were observed as there would be fewer $^{\bullet}OH$ radicals paired with an increased number of dye molecules. A similar trend is observed in many studies in the literatüre.[35,38]

Effect of fenton reagents

Fe^{2+} and H_2O_2 are used as reagents in the Fenton process. In the Fenton and Fenton-like oxidation process, the dosage of Fenton reagent plays a very important role in the degradation of organic matter and the overall cost of the process.[39] In the study, different H_2O_2 concentrations (10, 25, 50, 75, 100, 150, 200, 300, 400, 500 mg L^{-1}) and different Fe^{2+} concentrations (10, 25, 50, 75, 100, 200, 400 mg L^{-1} was applied to determine the effect of Fenton reagents on the degradation of RO16. Other conditions were: t 30 min., dye concentration 100 mg L^{-1}, pH 3 and Fe^{2+} 50 mg L^{-1} in H_2O_2 study, H_2O_2 100 mg L^{-1} in Fe^{2+} study. The RO16 degradation efficiencies for different reagent quantities are given in Figure 2.

With the addition of H_2O_2, RO16 degradation started to increase due to the increase in the $^{\bullet}OH$ concentration. However, the degradation efficiency did not change significantly when the increase in the amount of H_2O_2 continued. The degradation efficiencies for 10, 50, 100, 300 and 500 mg L^{-1} H_2O_2 were 73.21%, 88.04%, 97.21%, 97.4% and 97.46%, respectively. The continuation of the increase in degradation efficiency with increasing amount of H_2O_2 is due to the hydroxyl radical scavenging effect of H_2O_2 (Eqs.10-11)[40] and recombination of hydroxyl radicals (Eq. 12).[41]

$$H_2O_2 + {}^{\bullet}OH \rightarrow H_2O + HO_2^{\bullet} \quad (10)$$

$$HO_2^{\bullet} + {}^{\bullet}OH \rightarrow H_2O + O_2 \quad (11)$$

$$2\,{}^{\bullet}OH \rightarrow H_2O_2 \quad (12)$$

As can be seen in Figure 2, the degradation efficiency decreased as the amount of Fe^{2+} increased. The degradation efficiency was 97.77% in 10 mg L^{-1} Fe^{2+}, 96.33% in 50 mg L^{-1} Fe^{2+}, 80.36% in 200 mg L^{-1} Fe^{2+} and 60.68% in 400 mg L^{-1} Fe^{2+}. As the Fe^{2+} concentration increases, a higher amount of $^{\bullet}OH$ radicals will be produced. However, it is thought that such a situation adversely affects the oxidation capacity of excessive Fe^{2+} concentration. It is known that higher Fe^{2+} concentration may cause consumption of $^{\bullet}OH$ radicals and thus decrease the degradation efficiency (Eq. 13).[42]

$$Fe^{2+} + {}^{\bullet}OH \rightarrow Fe^{3+} + OH^{-} \quad (13)$$

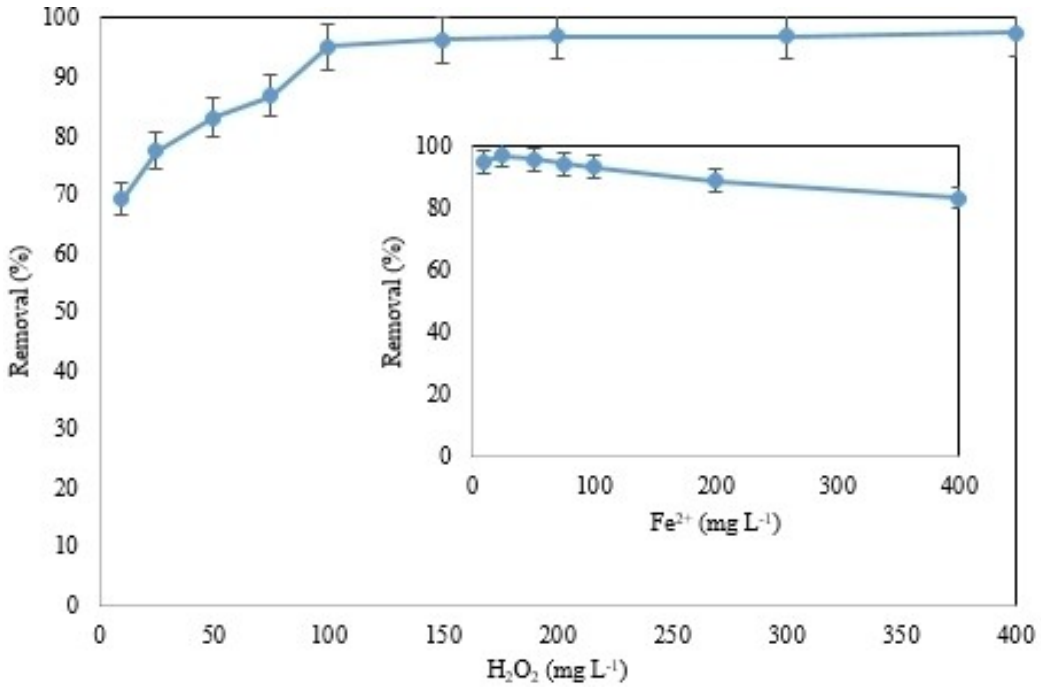

Figure 2. Effect of H_2O_2 and Fe^{2+} on RO16 degradation.

Reaction time

To determine the time dependent change of degradation, Analyzes were also performed at 5, 10, 15, 20, 25, 30, 45, 60, 90, 120, 180, 240 min. with keeping other conditions constant (Fe^{2+} 10 mg L^{-1}, H_2O_2 100 mg L^{-1}, pH 3 and concentrations of the dye 100 mg L^{-1}) (Figure 3).

Degradation occurred rapidly from the first minute of the reaction. Since the iron ion quickly catalyzes H_2O_2 in the first step of the reaction to form •OH, faster degradation occurred.[44]

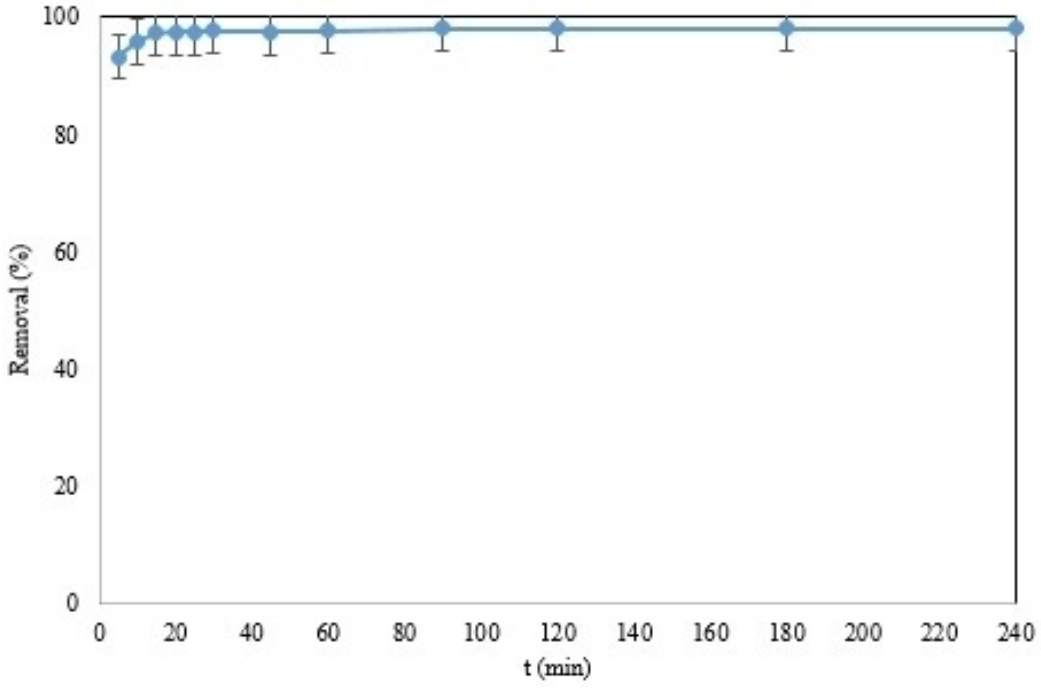

Figure 3. Effect of reaction time on the degratation.

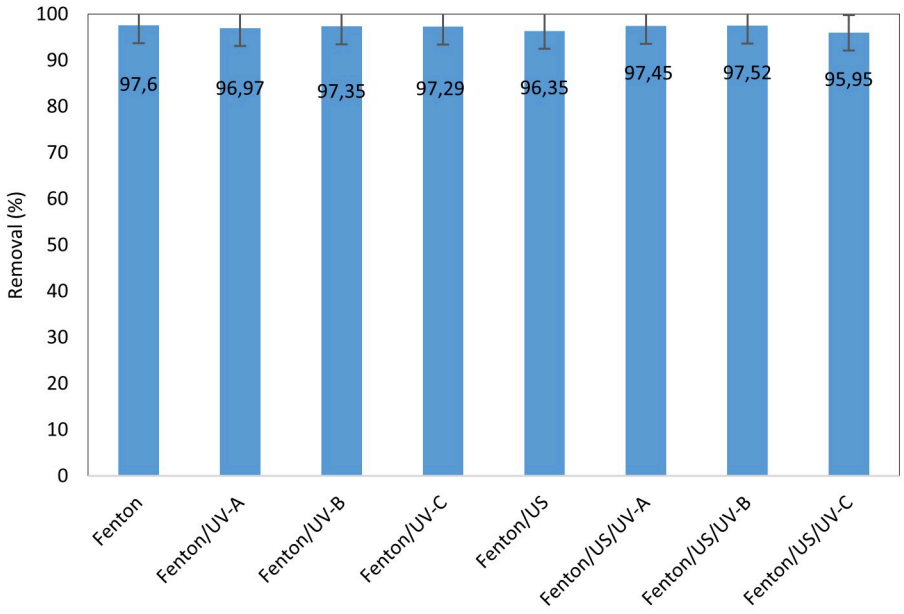

Figure 4. Effect of different Fenton like process on degratation.

After the 30th minute of the reaction, there was no significant change in the degradation efficiency and the optimum reaction time was determined as 30 minutes. While the degradation efficiency was 90.83% at the 5th minute of the reaction, it reached 97.5% at the 15th minute and 97.77% at the 30th minute. As the reaction continued, the efficiency recorded 98.23% at the 60th minute and 98.46% and 98.42% at the 120th and 240th minutes, respectively. At the start of the reaction, Equation (2) was quickly fulfilled. The •OH formed as a result of the reaction was used for the degradation of RO16. In the following time, since no additional Fenton reagent was added to the system, the degradation slowed down.

Comparative study in FP, P–FP, S–FP, S–P–FP

P–FP, sono Fenton process (S–FP) and S–P–FP applications were performed to examine the variation of RO16 degradation under different oxidation processes. The study was carried out using the optimum conditions obtained in the FP process (Fe^{2+} 10 mg L^{-1}, H_2O_2 100 mg L^{-1}, pH 3, t 30 min. and concentration 100 mg L^{-1}). In RO16 degradation, P-FP (Fe^{2+}/H_2O_2/UV–A/B/C), S–FP (Fe^{2+}/H_2O_2/US) and S–F–FP (Fe^{2+}/ H_2O_2/US/UV–A/B/C) was done to compare the individual and synergistic effects in the reactor. The degradation efficiency results of the dye for all processes are given in Figure 4.

As seen in Figure 4, no significant change in degradation efficiency was observed in different Fenton applications. In the Fenton study, high removal efficiencies were obtained in a very short time with the addition of reagents (97.77%). With the addition of UV (P–FP) RO16 degradation efficiency slightly increased. Efficiency for UV–A, UV–B and UV–C lamps was 98.78%, 98.31% and 98.22%, respectively. In S–FP, the degradation efficiency was 97.96%. No significant change was observed in S–P–FP, where the processes were used together. The highest synergy effect for degradation efficiency under different lamps in S–P–FP was obtained in Fenton/US/UV–C process (96.83%).

Kinetic constants

Kinetic analysis of RO16 degradation was performed using zeroth-order (Eq. 14), first-order (Eq. 15), and second-order (Eq. 16) kinetic models.[43] The resulted kinetic rate constants (k_0, k_1 and k_2) and correlation coefficients (R^2) of the equations are summarized in Table 1.

$$C = C_0 - k_0.t \quad (14)$$

Table 1. Kinetic constants in Fenton processes.

Process	0th. Order Kinetic		1st. Order Kinetic		2nd. Order Kinetic	
	k_0 (mg L.min^{-1})	R^2	k_1 (1 min^{-1})	R^2	k_2 (L mg.min^{-1})	R^2
Fenton	0.2017	0.51	0.0021	0.50	−2E-05	0.50
Fenton/UV-A	0.3592	0.71	0.0038	0.70	−4E-05	0.69
Fenton/UV-B	0.0867	0.90	0.0009	0.90	−9E-05	0.89
Fenton/UV-C	0.1531	0.72	0.0016	0.71	−2E-05	0.71
Fenton/US	1.1663	0.79	0.0139	0.78	−0.0002	0.76

$$lnC = lnC_0 - k_1.t \quad (15)$$

$$\frac{1}{C} = \frac{1}{C_0} + k_2.t \quad (16)$$

Here; C_0 initial concentration (mg L^{-1}); C is the concentration of RO16 (mg L^{-1}) at any time; k_0 (mg L min^{-1}), k_1 (1 min^{-1}) and k_2 (L mg min^{-1}) are the zeroth, first, and second order reaction kinetic constants, respectively; and t represents reaction time (min).

The highest correlation coefficient was obtained for the zeroth-order model ($R^2 > 0.90$). Therefore, RO16 degradation can be better explained by a zeroth-order kinetic model. Compared to other processes, an increase in k constants was observed in the S-FP application with US. The k_0 value was calculated as 0.2017 in the Fenton process and 0.3592, 0.0867 and 0.1531 in the UV–A, UV–B and UV–C processes, respectively, while it was calculated as 1.1663 in Fenton/US. The highest k_1 and k_2 constants were obtained in the Fenton/US process with 0.0139 and −0.0002, respectively. This can be explained by the relative increase in temperature with the use of US.[44]

The Result of DFT calculations regarding to reactant and product

Chemical reactivity analysis is to predict the behaviors of chemical systems against certain chemical species and under certain conditions. It is well-known that Conceptual Density Functional Theory is the branch aiming simply prediction of the chemical reactivities of atoms, ions and molecules of DFT. For that reason, we will start giving detailed information about popular electronic structure principles like Hard and Soft Acid-Base Principle,[45] Maximum Hardness Principle[46] and Minimum Polarizability Principle.[47] Chemical hardness[48,49] is known as the resistance against the polarization of electron cloud of atomic and molecular systems. This parameter is quite useful in the explaining the power and nature of the interactions between chemical systems. According to Hard and Soft Acid Base (HSAB) Principle of Pearson, Lewis acids and bases are classified into three groups as hard, soft and bonderline. HSAB Principle states that hard acids prefer to coordinate to hard bases and soft acids prefer to coordinate to soft bases because hard-hard and soft-soft interactions are mainly powerful interactions. Another electronic structure principle about chemical hardness concept is Maximum Hardness Principle highlighting the strong linkage between hardness and chemical stability. According to Maximum Hardness Principle,[50] "there seems to be a rule of nature that molecules arrange themselves so as to be as hard as possible" It can be easily understood that chemical hardness is a measure of the stability and hard chemical systems exhibit higher stability than soft ones. It is clear from the definition of chemical hardness concept that there is an inverse relation between chemical hardness and polarizability. The mathematical studies proving this inverse relation were published by Ghanty and Ghosh[51] and then, Chattaraj and Sengupta introduced the Minimum Polarizability Principle. This principle states that "the natural direction of evolution of any system is towards a state of minimum polarizability. Some researchers supported that dipole moment can be considered as a measure of the polarizability of the chemical systems. For that reason, we calculated dipole moment values also of studied chemical systems. In the light of Maximum Hardness and Minimum Polarizability Principles, Kaya[52] derived a new lattice energy equation and imparted to the science the Kaya's composite descriptor ($\eta/V_m^{1/3}$) based on chemical hardness and molar volume (V_m) of the chemical systems. In a recent paper, within the framework of Kaya's composite descriptor, Szentpaly and Kaya introduced Maximum Composite Hardness Rule. In Table 2, calculated quantum chemical descriptors for the products and reactants in degradation mechanism of RO16 dye. It can be seen from the calculated data that RO16 dye is quite reactive and exhibit good nucleophilic character and is a good electron donor because its low hardness and higher HOMO energy values. In some recently published research papers noted that •OH radical is a powerful electron acceptor.[53]

There is a fairly large difference in electronegativity values of •OH radical and RO16 dye. This situation implies that there will be a high rate of electron transfer between this radical and the dye. According to Electronegativity Equalization Principle,[54] when two systems with different electronegativities interact, electron transfer between them continues until their electronegativities are equal to each other. It can be noted Fenton-like Process is useful for the degradation of the dyes with low electronegativity, low hardness and high reactivity. Product atomic structure is given in Figure 5 and reactant atomic structure is given in Figure 6.

C–N bond break degradation mechanism

We analyzed the effect of the OH^- anion on the mechanism of covalent bond cleavage. Schematically, the potential energy profile for the reaction of anion with the RO16 dye and further degradation is shown in Figure 7. The OH^- anion covalently binds to the six-membered carbon ring of the dye, and then the process of isomerization and decay occurs through the transition state. In this case, the barrier for breaking the bond is

Table 2. Calculated quantum chemical descriptors for products and reactants.

$C_{20}H_{17}N_3Na_2O_{11}S_3$	Reactant	Product
HOMO (eV)	−1.850	−1.415
LUMO (eV)	−0.628	−0.514
η	1.222	0.901
σ	0.818	1.109
χ	1.239	0.964
ω_1	0.628	0.516
ω_2	0.950	0.807
ω^+	0.713	0.606
ω^-	1.952	1.571
$\Delta E_{back\text{-}donation}$	−0.305	−0.225
Dipole moment (Debye)	11.494	12.768

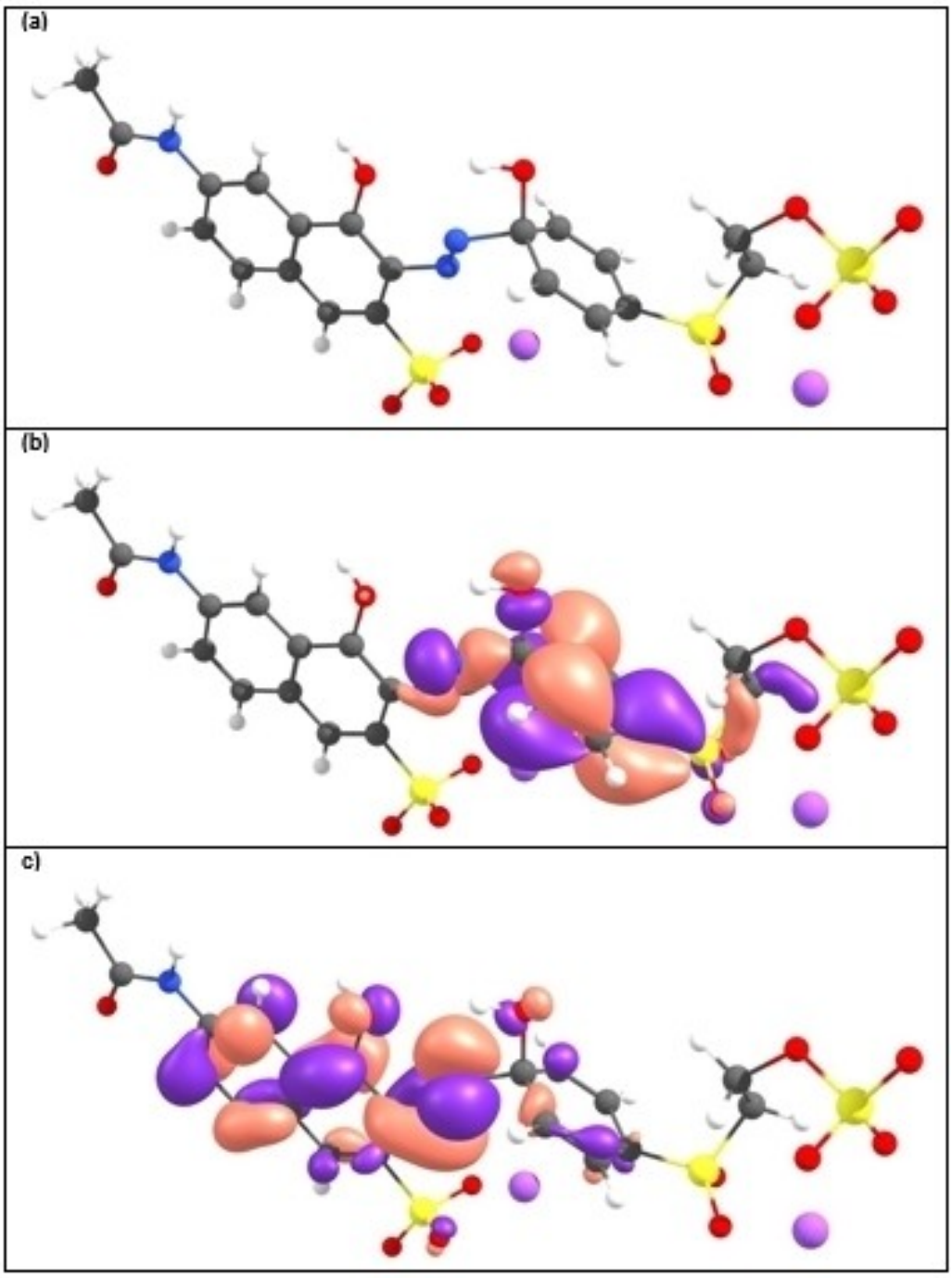

Figure 5. Reactant: atomic structure (a), HOMO (b), and LUMO (c).

quite high and amounts to 3.4 eV. As a result, the covalent C–N bond is broken and the anion covalently binds to nitrogen.

Conclusion

In this study, degradation of RO16 in aqueous solution was investigated by FP, P–FP, S–FP and S–P-FP applications under different experimental conditions. In order to determine the optimum conditions, variables such as pH, dye concentration, H_2O_2 dose, Fe^{2+} dose and reaction time were examined. Effective RO16 degradation was achieved by Fenton oxidation at conditions of 100 mg L^{-1} H_2O_2, 10 mg L^{-1} Fe^{2+}, 100 mg L^{-1} dye concentration, 3 pH and 30 minutes. While the degradation efficiency with FP was 97.77%, it reached 98.78%, 98.31% and 98.22% when UV–A, UV–B and UV–C lights were applied respectively. In the S-FP application, on the other hand, the degradation efficiency was 97.96%, while it decreased in the S–P-FP applications to 96.12%, 96.13% and 96.83% under

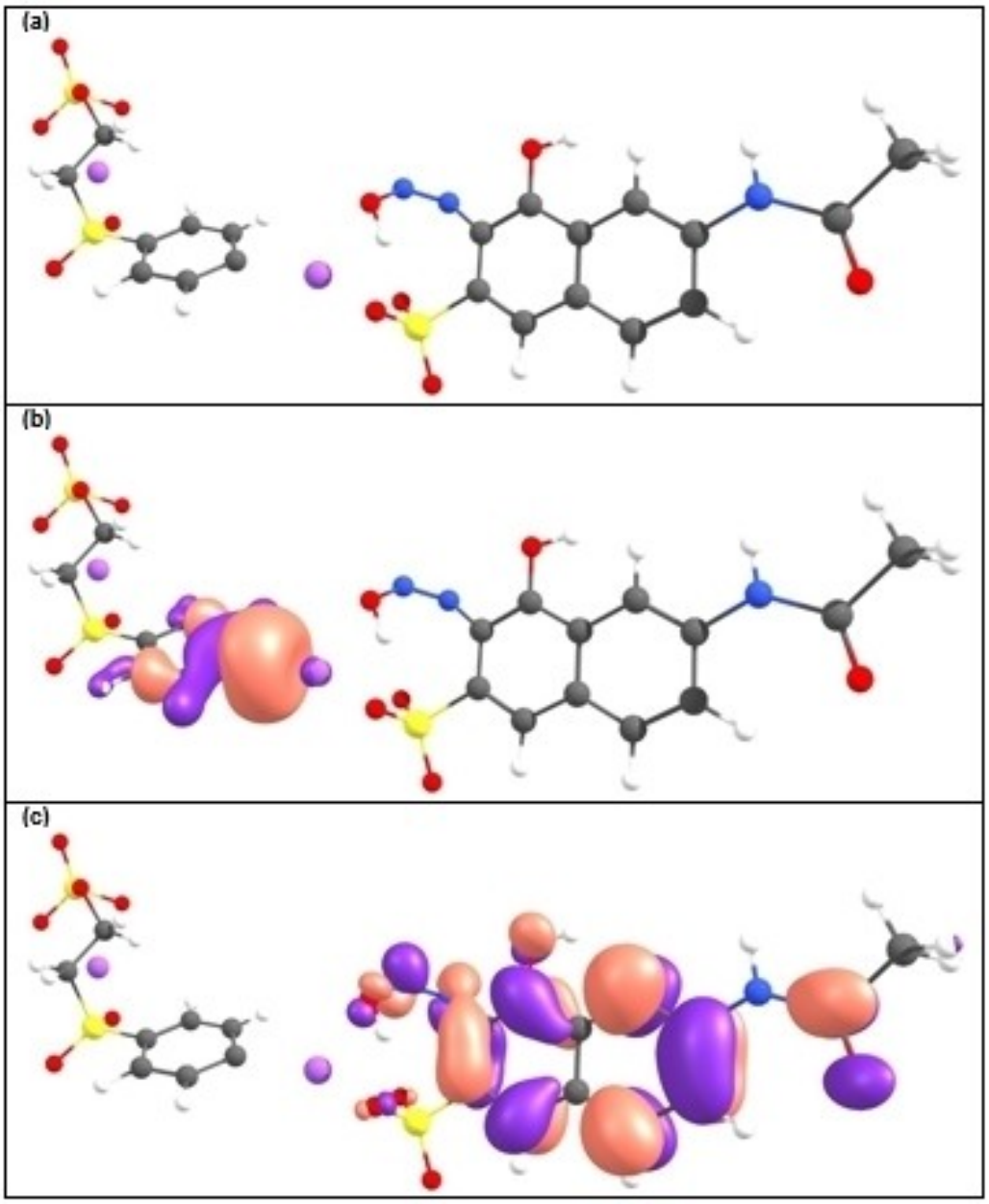

Figure 6. Product: atomic structure (a), HOMO (b), and LUMO (c).

different lamps (UV–A, UV–B and UV–C) respectively. In addition, in the kinetic study, it was determined that each process complies with the zeroth-order kinetics. The results revealed that RO16 degradation occurs in high efficiency by Fenton and Fenton-like processes. This process can be considered as a promising and effective method for removing the dye from water and wastewater. DFT calculations performing to see the degradation mechanism supported the Experimental observations.

Experimental Section

In the study, $FeSO_4.7H_2O$ (P 99%) and H_2O_2 (P 35%) stock solution was used as Fenton reagent. The pH of the solution was adjusted by adding 0.1 N NaOH and 0.1 N H_2SO_4. Fe^{2+} (as $FeSO_4.7H_2O$) and H_2O_2 were added to the solution, respectively. Experiments were carried out in a volume of 100 ml of liquid. UV–A (365 nm), UV–B (302 nm), UV–C (256 nm) light sources were used in the P-FP study. S–FP and S–P–FP studies were performed by applying ultrasound at a frequency of 40 kHz and a power of 180 watts. pH measurements were made with Adwa AD8000 brand device.

All chemicals used in this study were of analytical standard. Industrially used RO16 dye was used in the study. RO16 was provided by Sigma-Aldrich (Cas: 12225-83-1). Reactive dyes are

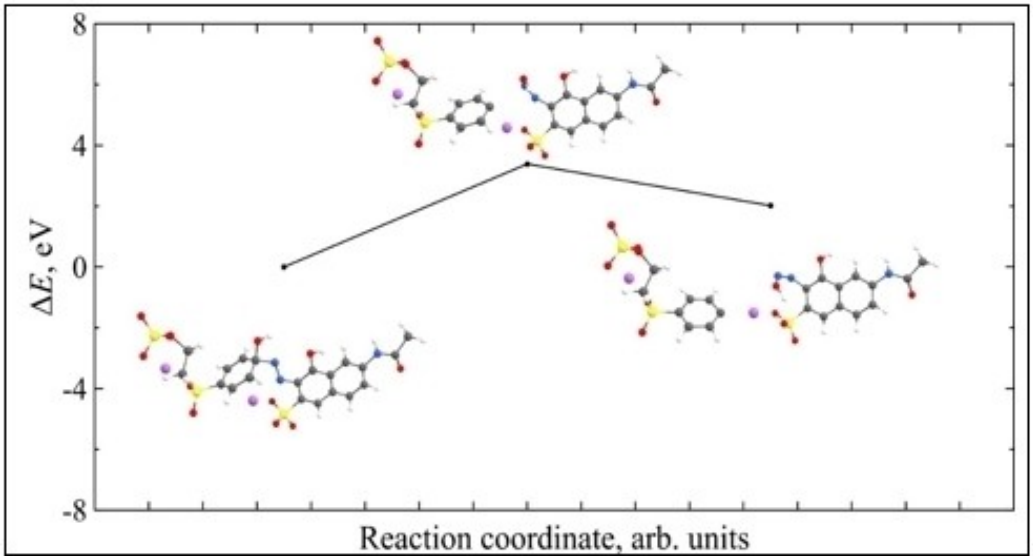

Figure 7. Potential energy profile for OH^- initiated degradation of RO16 dye via the C–N bond cleavage mechanism.

water-soluble, biodegradable, and stable because they form a strong complex.[4] The chemical formula of RO16, which is a reactive dye, is $C_{20}H_{17}N_3Na_2O_{11}S_3$[55] and its chemical structure is given in Table 3.[56] Values of the dye solution were determined with the Spectrophotometer (Merck Spectroquant Pharo 300) using a direct photometric method according to Standard Methods.[57] Experiments were repeated three times and mean values are presented. The standard deviation ($\leq$4%) and error bars are indicated in the figures.

The percent color removal at any time was obtained using Equation 17.

$$\%Removal = \frac{C_0 - C}{C_0} x100 \quad (17)$$

Here, C_0 is the initial concentration, C is the concentration at any time, and % Removal is the percent removal.

Details of density functional theory calculations

All calculations were performed using the Perdew-Burke-Ernzerhof (GGA-PBE) exchange-correlation functional[58] and 6-31G(d) electronic basic set[59] for all elements. We used the graphics processor-based TeraChem software.[60–63] Geometry optimization was carried out with the efficient geomeTRIC energy minimizer.[64] The dispersion corrections D3 proposed by Grimme[65] were also included to take into account the weak non-covalent interactions. Transition state was obtained in the frame of nudged elastic band (NEB) technique[66] as it was implemented in TeraChem. In the Conceptual Density Functional Theory (CDFT), electronic structure parameters are defined as the derivatives with respect to number of electrons at a constant external potential, electronic structure parameters are defined as the derivatives with respect to number of electrons (N) of total electronic energy (E) at a constant external potential, $\nu(r)$. In the given equations, $\nu(r)$ represents the constant external potential. CDFT presents some useful and simple formulae to compute well-known quantum chemical parameters such as chemical potential (μ), electronegativity (χ), hardness (η) and softness (σ). These mentioned formulae are given as (Eq. 18–20):[67]

Table 3. Chemical structure and absorbance of the dye.

Name	Chemical structure	λmax (nm)
RO16	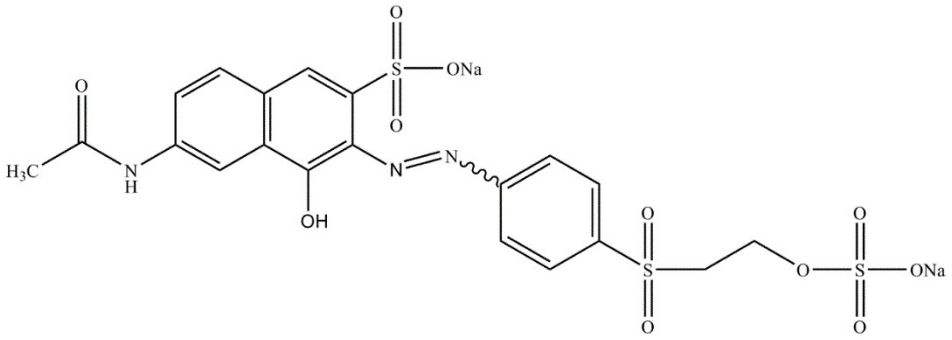	492

$$\mu = -\chi = \left[\frac{\partial E}{\partial N}\right]_{v(r)} \quad (18)$$

$$\eta = \left[\frac{\partial^2 E}{\partial N^2}\right]_{v(r)} \quad (19)$$

$$\sigma = 1/\eta \quad (20)$$

It is important to note that in the given formulae E and N stand for total electronic energy and total number of the electrons of the studied chemical system. It can be seen from the relations given above that electronegativity is the negative of the chemical potential. Within the framework of the finite differences approach, for the aforementioned descriptors, the following formulae (Eq. 21–23) based on ground state ionization energy (I) and electron affinity (A) of the studied chemical system.[68]

$$\mu = -\chi = -\left(\frac{I+A}{2}\right) \quad (21)$$

$$\eta = I - A \quad (22)$$

$$\sigma = \frac{1}{I-A} \quad (23)$$

Koopmans Theorem[69] is an alternative method for the approximately prediction of ground state ionization energy and electron affinities from frontier orbital energies. According to the theorem, ionization energy and electron affinity of any chemical system are approximately equal to the negative values of HOMO and LUMO orbital energies, respectively. In the light of this theorem, we can write the following relations (Eq. 24–25).

$$I = -E_{HOMO} \quad (24)$$

$$A = -E_{LUMO} \quad (25)$$

First electrophilicity index (ω_1) based on the absolute electronegativity and absolute hardness of atomic and molecules system is introduced by Parr, Szentpaly and Liu[70] and is given as (Eq. 26):

$$\omega_1 = (I+A)^2/8(I-A) = \chi^2/2\eta = \mu^2/2\eta \quad (26)$$

Recently, Szentpaly and Kaya[71] advocated that second electrophilicity index (ω_2) given via the following equation (Eq. 27) provides more compatible results with Minimum Electrophilicity Principle introduced by Chattaraj and coworkers.[72]

$$\omega_2 = I.A/(I-A) \quad (27)$$

To predict the electron donating power (ω^-) and electron accepting power (ω^+) of compounds, Gazquez and coworkers[73] derived the following equations (Eq. 28–29).

$$\omega^- = (3I+A)^2/(16(I-A)) \quad (28)$$

$$\omega^+ = (I+3A)^2/(16(I-A)) \quad (29)$$

Back-donation energy ($\Delta E_{back\text{-}donation}$) is a useful parameter giving information about the chemical reactivities of chemical systems. This parameter based on the absolute hardness of chemical system is calculated as (Eq. 30):

$$\Delta E_{back-donation} = -\eta/4 \quad (30)$$

Conflict of Interest

The authors declare no conflict of interest.

Keywords: degradation · DFT · fenton · RO16 · sono-photo-fenton

[1] B. Tanhaei, A. Ayati, M. Sillanpää, *Int. J. Biol. Macromol.* **2019**, *121*, 1126–1134.
[2] C. R. Holkar, A. J. Jadhav, D. V. Pinjari, N. M. Mahamuni, A. B. Pandit, *J. Environ. Manage.* **2016**, *182*, 351–366.
[3] L. Tan, M. He, L. Song, X. Fu, S. Shi, *Bioresour. Technol.* **2016**, *203, 287–294*.
[4] H. Zhang, J. Wang, K. Xie, L. Pei, A. Hou, *Dyes Pigm.* **2020**, *174*.
[5] D. A. Fungaro, S. I. Borrely, T. E. M. Carvalho, *Am. J. Environ. Prot.* **2013**, *1*, 1–9.
[6] F. P. Van Der Zee, S. Villaverde, *Water Res.* **2005**, *39, 1425–1440*.
[7] C. M. Rosu, M. Avadanei, D. Gherghel, M. Mihasan, C. Mihai, A. Trifan, A. Miron, G. Vochita, *Water Air Soil Pollut.* **2018**, *229(1), 1–18*.
[8] J. L. S. Duarte, L. Meili, L. M. Gomes, J. M. O. Melo, A. B. Ferro, M. G. Tavares, J. Tonholo, C. L. P. S. Zanta, *Chem. Eng. Process. Process Intensif.* **2019**, *142*, 107548.
[9] M. M. Martorell, H. F. Pajot, P. M. Ahmed, L. I. C. De Figueroa, *J. Environ. Sci.* (China). **2017**, *53*, 78–87.
[10] J. R. S. Carvalho, F. M. Amaral, L. Florencio, M. T. Kato, T. P. Delforno, S. Gavazza, *Chemosphere.* **2020**, *242, 125157*.
[11] L. Brahmi, F. Kaouah, S. Boumaza, M. Trari, *Appl. Water Sci.* **2019**, *9(8), 1–13*.
[12] V. Sharma, T. Shahnaz, S. Subbiah, S. Narayanasamy, *J. Polym. Environ.* **2020**, *28*, 2008–2019.
[13] N. N. A. Malek, A. H. Jawad, K. Ismail, R. Razuan, Z. A. ALOthman, *Int. J. Biol. Macromol.* **2021**, *189*, 464–476.
[14] E. Fathi, P. Gharbani, *Diamond Relat. Mater.* **2021**, *115*, 108346.
[15] C. Zhijiang, X. Ping, Z. Cong, Z. Tingting, G. Jie, Z. Kongyin, *Cellulose.* **2018**, *25*, 5123–5137.
[16] M. R. Sohrabi, A. Khavaran, S. Shariati, S. Shariati, *Arab. J. Chem.* **2017**, *10*, 3523–3531.
[17] R. G. L. Gonçalves, P. A. Lopes, J. A. Resende, F. G. Pinto, J. Tronto, M. C. Guerreiro, L. C. A. De Oliveira, W. De Castro Nunes, J. L. Neto, *Appl. Clay Sci.* **2019**, *179*, 105152.
[18] S. F. Azha, L. Sellaoui, E. H. Engku Yunus, C. J. Yee, A. Bonilla-Petriciolet, A. Ben Lamine, S. Ismail, *Chem. Eng. J.* **2019**, *361*, 31–40.
[19] M. Gągol, A. Przyjazny, G. Boczkaj, *Chem. Eng. J.* **2018**, *338*, 599–627.
[20] Y. Li, A. Zhang, *Chemosphere.* **2014**, *105*, 24–30.
[21] S. Yildiz, A. Cömert, *Int. J. Environ. Health Res.* **2020**, *30*, 89–104.
[22] N. Jaafarzadeh, A. Takdastan, S. Jorfi, F. Ghanbari, M. Ahmadi, G. Barzegar, *J. Mol. Liq.* **2018**, *256*, 462–470.
[23] I. Sirés, J. A. Garrido, R. M. Rodríguez, E. Brillas, N. Oturan, M. A. Oturan, *Appl. Catal. B* **2007**, *72*, 382–394.
[24] M. Hui Zhang, H. Dong, L. Zhao, D. Xi Wang, D. Meng, *Sci. Total Environ.* **2019**, *670*, 110–121.
[25] F. Ruscasso, I. Cavello, M. Butler, E. L. Loveira, G. Curutchet, S. Cavalitto, *Biores. Tech. Rep.* **2021**, *15*, 100726.
[26] A. L. Ahmad, S. W. Puasa, M. M. D. Zulkali, *Desalination* **2006**, *191*, 153–161.
[27] A. S. Abdulhameed, A. T. Mohammad, A. H. Jawad, *J. Cleaner Prod.* **2019**, *232*, 43–56.
[28] G. Kavitha, P. Subhapriya, V. Dhanapal, G. Dineshkumar, V. Venkateswaran, *Mater. Today: Proc.* **2021**, *45*, 7934–7938.
[29] F. D. Castro, J. P. Bassin, T. L. M. Alves, G. L. Sant'Anna, M. Dezotti, *International Journal of Environmental Science and Technology* **2021**, *18*, 1991–2010.

[30] M. Muruganandham, M. Swaminathan, *Dyes Pigm.* **2004**, *63*, 315–321.
[31] H. J. H. Fenton, *J. Chem. Soc. Trans.* **1894**, *65, 899–910*.
[32] A. Shokri, *Int. J. Ind. Chem.* **2018**, *9*, 295–303.
[33] K. Selvam, M. Muruganandham, M. Swaminathan, *Sol. Energy Mater. Sol. Cells.* **2005**, *89*, 61–74.
[34] E. G. Solozhenko, N. M. Soboleva, V. V. Goncharuk, *Water Res.* **1995**, *29*, 2206–2210.
[35] C. Bouasla, M. E. H. Samar, F. Ismail, *Desalination.* **2010**, *254*, 35–41.
[36] S. Bayar, M. Erdogan, *Appl. Ecol. Environ. Res.* **2019**, *17*, 1517–1529.
[37] C. D. Jonah, J. W. T. Spinks, R. J. Woods, *Radiat. Res.* **1990**, *124*, 378.
[38] G. Harichandran, S. Prasad, *Ultrason. Sonochem.* **2016**, *29*, 178–185.
[39] R. Saini, M. Kumar Mondal, P. Kumar, *Environ. Prog. Sustain. Energy.* **2017**, *36, 420–427*.
[40] K. Ntampegliotis, A. Riga, V. Karayannis, V. Bontozoglou, G. Papapolymerou, *J. Hazard. Mater.* **2006**, *136*, 75–84.
[41] C. Walling, *Acc. Chem. Res.* **1975**, *8*, 125–131.
[42] M. Pérez-Moya, M. Graells, L. J. Del Valle, E. Centelles, H. D. Mansilla, *Catal. Today.* **2007**, *124, 163–171*.
[43] S. Yildiz, A. Olabi, *Waste and Biomass Valorization.* **2021**, *12, 4419–4431*.
[44] J. C. Kotz, P. M. Treichel, J. R. Townsend, D. A. Treichel, *Chemistry & Chemical Reactivity* 9 Edition, **2015**.
[45] R. G. Pearson, *J. Am. Chem. Soc.* **1963**, *85, 3533–3539.*
[46] S. Kaya, C. Kaya, N. Islam, *Phys. Condens. Matter* **2016**, *485*, 60–66.
[47] P. K. Chattaraj, P. Fuentealba, P. Jaque, A. Toro-Labbé, *J. Phys. Chem. A.* **1999**, *103*, 9307–9312.
[48] S. Kaya, C. Kaya, *Mol. Phys.* **2015**, *113, 1311–1319*.
[49] S. Kaya, C. Kaya, *Comput. Theor. Chem.* **2015**, *1060*, 66–70.
[50] R. G. Pearson, *Acc. Chem. Res.* **1993**, *26*, 250–255.
[51] T. K. Ghanty, S. K. Ghosh, *J. Phys. Chem.* **1993**, *97*, 4951–4953.
[52] S. Kaya, C. Kaya, *Inorg. Chem.* **2015**, *54, 8207–8213*.
[53] A. Asghar, M. M. Bello, A. A. A. Raman, W. M. A. W. Daud, A. Ramalingam, S. B. M. Zain, *Heliyon.* **2019**, *5(9)*, e02396.
[54] S. Kaya, C. Kaya, *Comput. Theor. Chem.* **2015**, *1052*, 42–46.
[55] B. Karagozoglu, M. Tasdemir, E. Demirbas, M. Kobya, *J. Hazard. Mater.* **2007**, *147*, 297–306.
[56] F. Marrakchi, W. A. Khanday, M. Asif, B. H. Hameed, *Int. J. Biol. Macromol.* **2016**, *93*, 1231–1239.
[57] APHA (American Public Health Association), Standard Methods for the Examination of Water and Wastewater, Stand. Methods. **1998**, *541*.
[58] J. P. Perdew, K. Burke, M. Ernzerhof, *Phys. Rev. Lett.* **1996**, *77*, 3865–3868.
[59] M. M. Francl, W. J. Pietro, W. J. Hehre, J. S. Binkley, M. S. Gordon, D. J. DeFrees, *J. Chem. Phys.* **1982**, *77*, 3654–3665.
[60] I. S. Ufimtsev, T. J. Martinez, *J. Chem. Theory Comput.* **2009**, *5*, 2619–2628.
[61] A. V. Titov, I. S. Ufimtsev, N. Luehr, T. J. Martinez, *J. Chem. Theory Comput.* **2013**, *9*, 213–221.
[62] J. Kästner, J. M. Carr, T. W. Keal, W. Thiel, A. Wander, P. Sherwood, *J. Phys. Chem. A.* **2009**, *113*, 11856–11865.
[63] T. P. M. Goumans, C. R. A. Catlow, W. A. Brown, J. Kästner, P. Sherwood, *Phys. Chem. Chem. Phys.* **2009**, *11*, 5431–5436.
[64] L. P. Wang, C. Song, *J. Chem. Phys.* **2016**, *144*, 214108.
[65] S. Grimme, J. Antony, S. Ehrlich, H. Krieg, *J. Chem. Phys.* **2010**, *132*, 154104.
[66] G. Henkelman, B. P. Uberuaga, H. Jónsson, *J. Chem. Phys.* **2000**, *113*, 9901–9904.
[67] Conceptual Density Functional Theory and Its Application in the Chemical Domain, **2018**.
[68] G. Serdaroğlu, S. Kaya, R. Touir, *J. Mol. Liq.* **2020**, *319*, 114108.
[69] T. Koopmans, *Physica.* **1934**, *1*, 104–113.
[70] R. G. Parr, L. V. Szentpály, S. Liu, *Electrophilicity index* **1999**, *121*, 1922–1924.
[71] L. Von Szentpaly, S. Kaya, N. Karakus, *J. Phys. Chem. A.* **2020**, *124*, 10897–10908.
[72] S. Pan, M. Solà, P. K. Chattaraj, *J. Phys. Chem.* A. **2013**, *117*, 1843–1852.
[73] J. L. Gázquez, A. Cedillo, A. Vela, *J. Phys. Chem. A.* **2007**, *111*, 1966–1970.

Submitted: June 14, 2022
Accepted: December 2, 2022